Monthly Notices of the ROYAL ASTRONOMICAL SOCIETY

MNRAS **490,** 1186–1201 (2019) doi:10.1093/mnras/stz2649
Advance Access publication 2019 September 21

A predicted correlation between age gradient and star formation history in FIRE dwarf galaxies

Andrew S. Graus,[1,2]★ James S. Bullock,[2] Alex Fitts,[1] Michael C. Cooper,[2] Michael Boylan-Kolchin,[1] Daniel R. Weisz,[3] Andrew Wetzel,[4] Robert Feldmann,[5] Claude-André Faucher-Giguère,[6] Eliot Quataert,[3] Philip F. Hopkins[7] and Dušan Kereš[8]

[1]*Department of Astronomy, The University of Texas at Austin, 2515 Speedway Stop C1400, Austin, TX 78712, USA*
[2]*Center for Cosmology, Department of Physics and Astronomy,4129 Reines Hall, University of California Irvine, CA 92697, USA*
[3]*Department of Astronomy and Theoretical Astrophysics Center, University of California, Berkeley, Berkeley, CA 94720, USA*
[4]*Department of Physics, University of California, Davis, CA 95717, USA*
[5]*Institute for Computational Science, University of Zurich, Zurich CH-8057, Switzerland, UK*
[6]*Department of Physics and Astronomy and CIERA, Northwestern University, 2145 Sheridan Road, Evanston, IL 60208, USA*
[7]*TAPIR, Mailcode 350-17, California Institute of Technology, Pasadena, CA 91125, USA*
[8]*Department of Physics, Center for Astrophysics and Space Science, University of California at San Diego, 9500 Gilman Drive, La Jolla, CA 92093, USA*

Accepted 2019 September 17. Received 2019 August 18; in original form 2018 December 19

ABSTRACT

We explore the radial variation of star formation histories (SFHs) in dwarf galaxies simulated with Feedback In Realistic Environments (FIRE) physics. The sample contains 26 field dwarf galaxies with $M_{\rm star} = 10^5$–10^9 M$_\odot$. We find age gradients are common in our dwarfs, with older stars dominant at large radii. The strength of the gradient correlates with overall galaxy age such that earlier star formation produces a more pronounced gradient. The relation between formation time and strength of the gradient is driven by both mergers and star formation feedback. Mergers can both steepen and flatten the age gradient depending on the timing of the merger and SFHs of the merging galaxy. In galaxies without significant mergers, feedback pushes stars to the outskirts. The strength of the age gradient is determined by the subsequent evolution of the galaxy. Galaxies with weak age gradients constantly grow to $z = 0$, meaning that young star formation occurs at a similar radius to which older stars are heated to. In contrast, galaxies with strong age gradients tend to maintain a constant half-mass radius over time. If real galaxies have age gradients as we predict, stellar population studies that rely on sampling a limited fraction of a galaxy can give a biased view of its global SFH. Central fields can be biased young by Gyrs while outer fields are biased old. Fields positioned near the 2D half-light radius will provide the least biased measure of a dwarf galaxy's global SFH.

Key words: galaxies: dwarf – galaxies: formation – Local Group – cosmology: theory.

1 INTRODUCTION

A key question in galaxy formation is to understand how stellar mass builds up in galaxies over time. Observed colour–magnitude diagrams (CMDs) together with sophisticated stellar population synthesis models provide a powerful approach to measure the star formation histories (SFHs) of galaxies and directly answer this question for certain systems (Dolphin 2002; Tolstoy, Hill & Tosi 2009; Monelli et al. 2010; Walmswell et al. 2013; Cole et al. 2014; Weisz et al. 2014a; Monelli et al. 2016; Makarova et al. 2017; Skillman et al. 2017). This technique is particularly useful for understanding dwarf galaxies in the local Universe, where precise photometry for populations of individual stars enables the construction of accurate CMDs.

The inferred SFHs of local dwarf galaxies have revealed much about the nature of galaxy formation on small scales. For example, ultrafaint dwarfs appear to be almost universally old (Brown et al. 2014; Weisz et al. 2015), lending support to the idea that these objects had their star formation quenched by reionization (Efstathiou 1992; Bullock, Kravtsov & Weinberg 2000; Ricotti & Gnedin 2005; Rodriguez Wimberly et al. 2018). Most larger dwarf galaxies, on the other hand, cease star formation only when they are within the virial radius of a larger galaxy (e.g. the Milky Way or

★ E-mail: agraus@utexas.edu

M31), a result that provides a useful means to constrain models of environmental quenching (Geha et al. 2012; Fillingham et al. 2015, 2016; Gallart et al. 2015; Weisz et al. 2015; Wetzel, Tollerud & Weisz 2015).

A further application of Local Group dwarf SFHs is to study the high-redshift universe. Accurate measurements of SFHs allow us to extrapolate galaxy properties back in time and to place constraints on high-redshift luminosity and stellar mass functions (Boylan-Kolchin, Bullock & Garrison-Kimmel 2014; Weisz, Johnson & Conroy 2014b; Boylan-Kolchin et al. 2015; Graus et al. 2016). More generally, comparisons between SFHs from simulated and observed galaxies provide important tests for cosmological models of galaxy formation. Such studies suggest that strong stellar feedback is essential for explaining the dwarf galaxy population (e.g. Di Cintio et al. 2014; Dutton et al. 2016; Read, Agertz & Collins 2016; Sawala et al. 2016; Garrison-Kimmel et al. 2017).

Strong stellar feedback not only regulates star formation, it also can change structural properties of the galaxy. For example, feedback from supernovae has been shown to create cores in the dark matter halo profiles of simulated dwarf galaxies (e.g. Pontzen & Governato 2012; Chan et al. 2015; Oñorbe et al. 2015; Fitts et al. 2017). This is important as it could be a key component in solving small-scale problems with ΛCDM (Bullock & Boylan-Kolchin 2017). For example, the cusp-core problem (Flores & Primack 1994; Moore 1994), where observations of some dwarf galaxies are best fit by cored dark matter density profiles, in contrast to dark matter only simulations in which haloes have NFW cusps. This can also help alleviate the 'too big to fail' problem (Boylan-Kolchin, Bullock & Kaplinghat 2011), where the most massive subhaloes of Milky Way-like haloes appear too dense to host the largest galaxies seen observationally in ΛCDM.

The same feedback episodes that alter the dynamics of dissipationless dark matter in haloes can also affect the collisionless stars in galaxies. Indeed, we expect the dark matter and stars to respond dynamically to feedback-induced potential fluctuations in a qualitatively similar manner, given that both behave as (effectively) collisionless fluids. Such an effect was investigated by El-Badry et al. (2016), who used the FIRE-1[1] simulations to show that simulated dwarf galaxies with strong stellar feedback have large fluctuations in their effective stellar radii over time (see also Stinson et al. 2009). This effect can eventually lead to an overall median age gradient where young stars form in the centre of the galaxy and old stars are preferentially found in the outskirts. Qualitatively, this agrees with the observed age and metallicity gradients seen in most dwarf galaxies locally, where younger (more metal-rich) stars lie in the centre and older (more metal-poor) stars in the outskirts (Battaglia et al. 2006; Faria et al. 2007; Beccari et al. 2014; McMonigal et al. 2014; del Pino, Aparicio & Hidalgo 2015; Santana et al. 2016; Kacharov et al. 2017; McQuinn et al. 2017; Okamoto et al. 2017; Cicuéndez et al. 2018; Cicuéndez & Battaglia 2018).

Age and metallicity gradients could potentially be relevant for the measurement of SFHs, as a spread in age with position could lead to biases in the observed SFHs relative to the true SFH. Specifically, if a CMD study relies on a field that is small compared to the galaxy's area on the sky, the inferred SFH might not represent the global history of the galaxy. While the simulations studied in El-Badry et al. (2016) included enough dwarf galaxies to study the origin of population gradients (four systems with $M_{\rm star} = 10^6$–10^9 M$_\odot$) the sample was not large enough to explore trends and potential observational biases associated with this effect. Here, we use a sample of 26 dwarf galaxy simulations with stellar masses from 10^5 to 10^9 M$_\odot$, including 9 presented in Fitts et al. (2017) and 17 introduced here, all run with the GIZMO code (Hopkins 2015)[2] and the FIRE-2 feedback implementation (Hopkins et al. 2018). Our aim is to study the spatial variation in SFHs over our entire suite of simulations, to search for correlations between the SFH gradient and other observables, and to use our simulations to explore the biases in SFHs that could arise from small-field CMD studies of local galaxies.

In Section 2, we discuss the simulations and our methodology for measuring variations in SFHs. Section 3 presents our predictions for SFHs, how they vary with radius, and shows that the strength of the gradient increases with galaxy age. In Section 4, we discuss the origins of these variations, and what the gradients imply for interpreting current and future observations of Local Group dwarf galaxies.

2 SIMULATIONS AND METHODS

The simulations used in this work were run using the multimethod gravity + hydrodynamics code GIZMO (Hopkins 2015) and utilize the the FIRE-2 feedback implementation (Hopkins et al. 2018). We specifically use a mesh-free Lagrangian Godunov (MFM) method that is second-order accurate and maintains many of the advantages of traditional SPH codes, while avoiding some of the traditional pitfalls of classic SPH codes such as accurate capturing of shocks, and general treatment of fluids, for which grid-based codes have traditionally been better. The simulations include star formation in dense molecular gas that is self-shielding, and Jeans-unstable (Krumholz & Gnedin 2011). We also include cooling and heating from an ionizing background (Faucher-Giguère et al. 2009), along with photo-heating and radiation pressure from stellar sources including feedback from OB stars and AGB mass-loss. We also include Type Ia and Type II supernovae. All the stellar physics is calculated assuming each star particle is a simple stellar population with a Kroupa (2001) initial mass function. Furthermore, we include turbulent diffusion of metals (Hopkins 2017; Su et al. 2017), which provides for a better match to observed metallicity distributions of Local Group dwarf galaxies (Escala et al. 2018).

Our sample includes 9 of the dwarf galaxies introduced in Fitts et al. (2017) along with an additional suite of 17 isolated dwarf galaxies presented for the first time here. Table 1 presents an overview of the simulations along with adopted names. The Fitts et al. (2017) dwarfs (named m10b-m) were choose to form in haloes of mass $M_{\rm v} \simeq 10^{10}$ M$_\odot$ at $z = 0$ and were simulated with dark matter particle masses of $m_{\rm dm} = 2500$ M$_\odot$ and initial gas particle masses of $m_{\rm g} = 500$ M$_\odot$. These dwarf galaxies form between 10^5 and 10^7 M$_\odot$ in stars, where the mass of a star particle is initially the same as a gas particle. The second set of simulations (named m10xa-i) includes 17 haloes with $M_{\rm v} = 0.1$–1×10^{11} M$_\odot$ each run with dark matter masses of $m_{\rm dm} = 20\,000$ M$_\odot$ and initial gas particle masses of $m_{\rm g} = 4\,000$ M$_\odot$. These more massive dwarfs form between 10^7 and 10^9 M$_\odot$ of stars and are similar to the most massive dwarf galaxies seen in the Local Group. For the new suite of simulations, we name the most massive halo after the simulation itself (m10xa-i). Lower mass haloes from the same simulation are designated by the simulation name followed by a capital latter (A, B, C, etc.).

[1] http://fire.northwestern.edu

[2] http://www.tapir.caltech.edu/ phopkins/Site/GIZMO.html

Table 1. Table of properties of the simulated galaxies used in this work at $z = 0$. (1) stellar mass, (2) halo mass, (3) maximum circular velocity, (4) mean 2D half-light radius over all projections; (5) lookback time to the formation of 50% of stars within 10% of the virial radius of the halo; (6) lookback time to the formation of 90% of stars within 10% of the virial radius of the halo; (7) and (8) age gradients defined in equation (1); (9) the fraction of stars that were brought in via mergers.

Halo	$M_{\rm star}$ ($M_\odot$) (1)	$M_{\rm halo}$ ($M_\odot$) (2)	$V_{\rm max}$ (km s^{-1}) (3)	$R_{1/2}$ (kpc) (4)	t_{50} (Gyr) (5)	t_{90} (Gyr) (6)	γ_{50} (Gyr/$R_{1/2}$) (7)	γ_{90} (Gyr/$R_{1/2}$) (8)	$f_{\rm acc}$ (9)
m10xa	7.64e07	1.87e10	45.26	2.23	6.08	1.06	− 0.3	0.1	0.02
m10xb	3.29e07	2.22e10	42.78	1.73	4.23	0.85	− 0.5	− 0.6	0.02
m10xc	1.19e08	3.22e10	48.31	2.25	6.55	1.00	− 2.2	− 0.3	0.01
m10xc_A	8.46e06	8.52e09	35.03	1.24	10.89	4.55	− 2.4	− 4.0	0.01
m10xd	6.81e07	3.86e10	53.51	2.60	4.04	1.72	− 0.5	− 1.0	0.13
m10xd_A	1.44e07	2.40e10	38.52	1.38	1.63	0.469	0.0	− 0.1	0.07
m10xe	3.26e08	4.57e10	56.17	2.93	6.13	1.72	− 1.5	− 0.9	0.01
m10xe_A	3.64e06	1.36e10	35.74	0.90	8.50	1.17	− 3.2	− 1.4	0.00
m10xe_B	1.28e07	1.12e10	38.15	1.31	8.75	4.76	− 1.8	− 2.9	0.01
m10xe_C	1.84e07	1.04e10	34.43	2.11	7.08	1.66	− 0.9	− 0.6	0.02
m10xe_D	3.61e06	8.88e09	34.13	2.43	9.62	3.82	0.1	− 0.9	0.00
m10xf	1.28e08	5.21e10	58.47	2.30	7.38	1.93	− 2.6	− 2.6	0.04
m10xg	4.61e08	6.20e10	65.75	2.78	7.59	2.00	− 2.3	− 1.3	0.05
m10xg_A	1.88e07	1.53e10	40.31	1.51	5.11	0.86	− 1.3	− 0.3	0.01
m10xh	5.4e08	7.44e10	68.10	4.15	3.65	0.55	0.9	0.2	0.16
m10xh_A	4.97e07	1.47e10	38.80	2.19	5.68	1.39	− 1.6	− 0.7	0.02
m10xi	4.48e08	7.58e10	64.35	3.56	6.03	2.71	− 2.1	− 1.6	0.03
Fitts et al. (2017)									
m10b	4.65e + 05	9.29e + 09	31.51	0.24	2.54	0.65	− 0.1	− 0.1	0.05
m10c	5.75e + 05	8.92e + 09	31.40	0.25	4.07	0.96	− 1.8	− 0.6	0.00
m10e	1.98e + 06	1.02e + 10	31.44	0.43	5.63	1.02	− 0.9	− 0.6	0.04
m10f	4.11e + 06	8.56e + 09	35.66	0.52	11.96	5.33	− 4.0	− 4.2	0.29
m10h	7.80e + 06	1.28e + 10	37.98	0.58	11.64	2.52	− 4.6	− 2.5	0.03
m10j	9.74e + 06	1.10e + 10	37.98	0.50	11.51	3.94	− 2.5	− 2.7	0.05
m10k	1.04e + 07	1.15e + 10	38.22	0.85	10.74	4.18	− 2.5	− 2.5	0.07
m10l	1.30e + 07	1.06e + 10	37.62	0.54	10.76	3.34	− 2.1	− 3.0	0.01
m10m	1.44e + 07	1.15e + 10	38.51	0.69	9.86	3.76	− 2.1	− 3.1	0.03

The stellar mass versus halo mass and stellar mass versus $V_{\rm max}$ relation for the simulated galaxies used in this work are shown in Fig. 1.

Furthermore, in Fig. 1 we provide a comparison between our theoretical galaxy sample and observed dwarf galaxies in the Local Volume. First, we show a comparison between the half-mass radii of the observed galaxies and the half-mass radii of the theoretical sample. Data for the observed sample of galaxies was taken from the SPARC sample Lelli et al. (2016), where the half-mass radii were computed from the 3.6 μm luminosities by assuming a fixed stellar mass-to-light ratio of 0.5 $M_\odot/L_\odot$, as assumed in Lelli et al. (2016). The rest of the observational sample was taken from many different sources, a full list of which can be found in Appendix B. At fixed stellar mass, our galaxies appear to be reasonably within the sizes of observed galaxies, but potentially too large on average. One part of this could be the impact of resolution, as seen in previous FIRE simulations (Chan et al. 2018; Wheeler et al. 2018). Higher resolution systems tend to have lower stellar masses and smaller sizes. This can also be seen in the sample of dwarf galaxies used in this work explicitly. The Fitts et al. (2017) sample is higher resolution than the galaxies presented first in this work, and seem to have noticeably smaller sizes at fixed stellar mass. Additionally, FIRE-2 appears unable to produce some of the very compact dwarf galaxies that are seen observationally. The bottom right panel of Fig. 1 compares the velocity dispersions of observed dwarf galaxies to that from our theoretical sample. The theoretical velocity dispersions are 1D velocity dispersion calculated by assuming $\sigma_* = \sigma_{*,\,3D}/\sqrt{3}$. In this space, it appears as thought FIRE-2 is able to reproduce the velocity dispersions of dwarf galaxies quite well.

All of these simulations are cosmological zoom-in simulations (e.g. Katz & White 1993; Oñorbe et al. 2014) with initial conditions generated using the `MUSIC` initial conditions generator (Hahn & Abel 2011). Halo finding in the simulation was done using a combination of the `Rockstar` halo finder (Behroozi, Wechsler & Wu 2013a), and the Amiga Halo Finder (`AHF` Knollmann & Knebe 2009) to verify the properties of the haloes and galaxies in this suite including the masses and centres of the haloes and galaxies. Furthermore, we track the evolution of galaxies and haloes back in time by constructing full merger trees for all the systems in our sample using `consistent-trees` (Behroozi et al. 2013b). One final note is that the two sets of simulations have slightly different cosmologies with the Fitts et al. (2017) sample having cosmological parameters: $H_0 = 71.0$ km s^{-1} Mpc^{-1}, $\Omega_{\rm m} = 0.266$, $\Omega_{\rm b} = 0.044$, $\Omega_\Lambda = 0.734$, while for the new sample of large galaxies the cosmological parameters are $H_0 = 70.2$ km s^{-1} Mpc^{-1}, $\Omega_{\rm m} = 0.272$, $\Omega_{\rm b} = 0.0455$, $\Omega_\Lambda = 0.728$.

3 RESULTS

3.1 SFH gradients

Fig. 2 shows examples of the SFH gradients for three galaxies in the sample (m10xb, m10xe, m10l) arranged from top to bottom

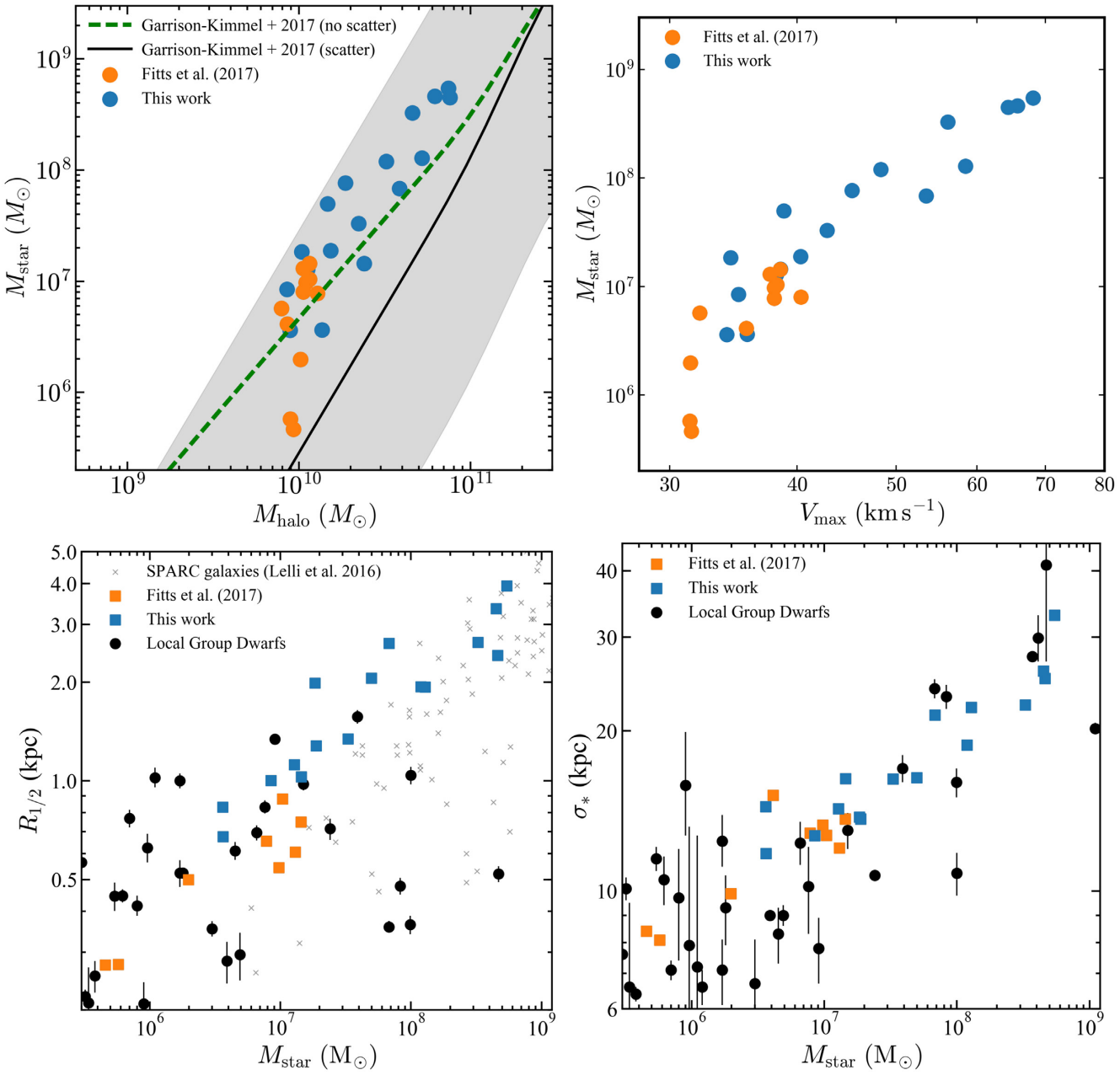

Figure 1. Top-left: Stellar mass versus halo mass for the simulated dwarf galaxies used in this paper. The dashed and solid lines show abundance matching relations presented in Garrison-Kimmel et al. (2017), which show the best-fitting abundance matching relation for the Milky Way satellites given zero scatter (green) and 2 dex of scatter (black line with the gray band). Top-right: and stellar mass versus halo maximum circular velocity. Bottom-left: Comparison of half-mass radii for the simulated galaxy sample to the half-mass radii of observed galaxies. Bottom-right: Stellar mass versus stellar velocity dispersion, once again compared to data. The Local Group data is composed of observations of large galaxies from the SPARC sample Lelli, McGaugh & Schombert (2016), and galaxies within the Local Group from McConnachie (2012) and various other sources (see Appendix B for a complete list). The mass of the SPARC galaxies was calculated assuming a constant mass-to-light ratio of 0.5 $M_\odot/L_\odot$ as in Lelli et al. (2016).

by strength of the gradient. The images in the left column show circularly averaged age maps seen in projection along an arbitrary axis. The size scale is normalized by the projected (2D) half-mass radius of the galaxy $R_{1/2}$. The stars are then binned into 10 bins within 1.5 × $R_{1/2}$ such that the number of stars is equal in each bin. The colour code maps to the median age of stars in each radial bin. The panels on the right show the SFHs within 10 radial bins, now colour-coded by the bin radius. The top row shows one of the weakest SFH gradients in our sample, while the bottom row shows one of the strongest. Note that m10l with a strong gradient is also the oldest of the three (with the longest lookback time for median star formation) while m10xb is the youngest overall. We show below that a trend between global age and overall SFH gradient is seen throughout our sample.

Fig. 3 quantifies the age gradients for the same galaxies illustrated in Fig. 2. The two colours correspond to different characteristic ages: blue shows the lookback time to when stars in a projected radial bin first reached 50 per cent of their final stellar mass (t_{50}); orange

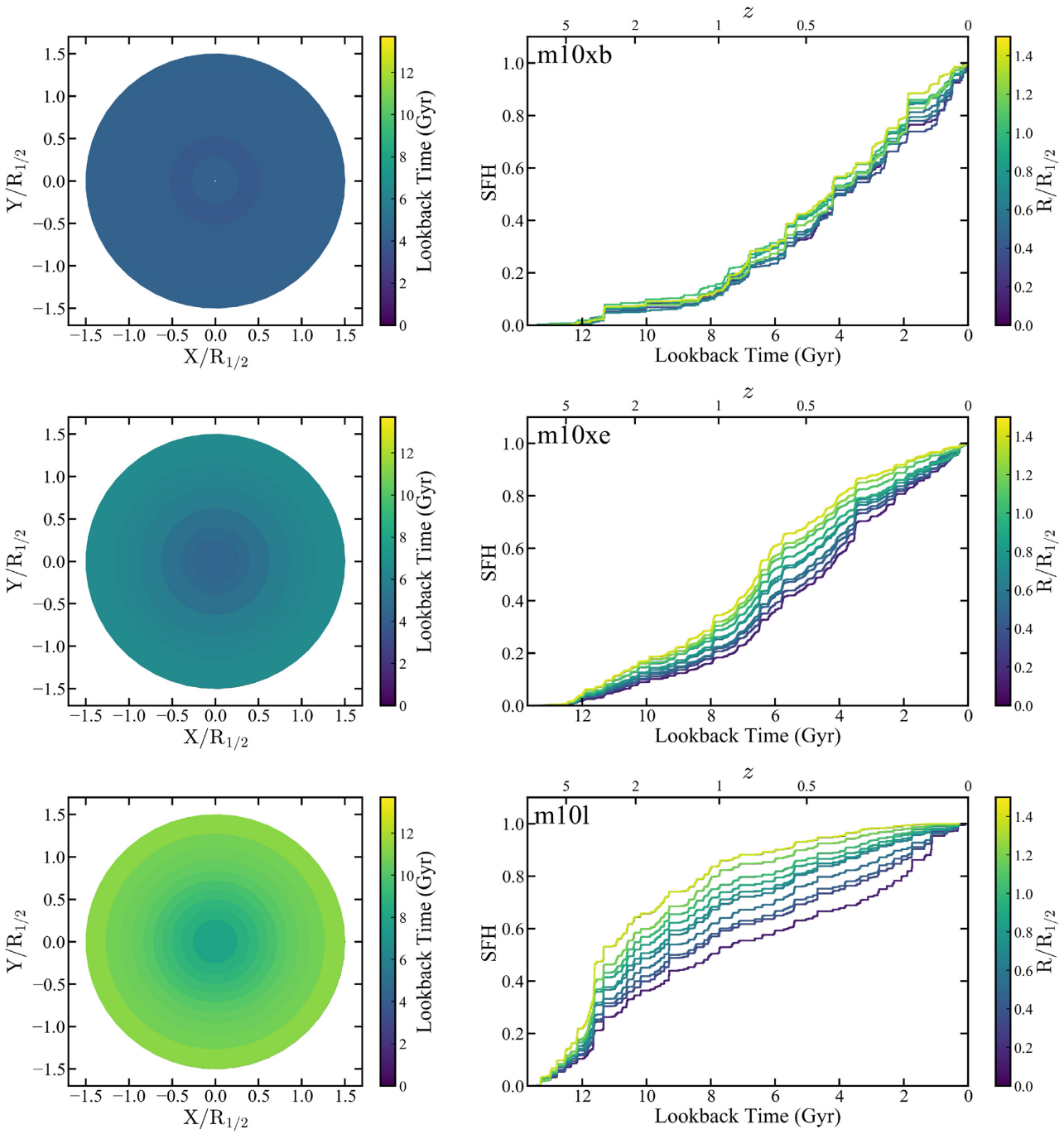

Figure 2. Example SFH gradients in three galaxies. Left: Map of median stellar age in projected radial bins normalized by the 2D half-mass radius. The colour bar maps to age (lookback time to formation) as indicated, with yellow corresponding to older stars and purple to younger stars. Right: The cumulative SFH within each projected radial bin coloured by the distance of the bin from the centre of the galaxy as indicated by the colour bar on the right. Note that the youngest galaxy has the least pronounced SFH gradient on the upper right. The oldest galaxy has the strongest SFH gradient on the lower right. The bins are fixed to be circular, however we note that the resulting gradients do not change significantly if we allow the contours to be elliptical.

shows the lookback time to the formation of 90 per cent of the final stellar mass (t_{90}). Stated another way, t_{50} is the median age of the stars at a given radius and t_{90} is the 90th percentile age of stars at a given radius. The solid blue (orange) line shows the median values of t_{50} (t_{90}) computed at a given projected radius over 100 random viewing angles for each galaxy. The shaded regions show the 99th percentile ranges over all projections. We quantify the gradients by measuring the radial variation in t_{50} and t_{90} as:

$$\gamma_{50} = \frac{\Delta t_{50}}{\Delta R/R_{1/2}}; \qquad \gamma_{90} = \frac{\Delta t_{90}}{\Delta R/R_{1/2}}. \tag{1}$$

Note that the gradients are normalized to the half-mass radius and have units of Gyr (per $R_{1/2}$). The value of the slope tells us simply how much older the stars at the half-mass radius are than

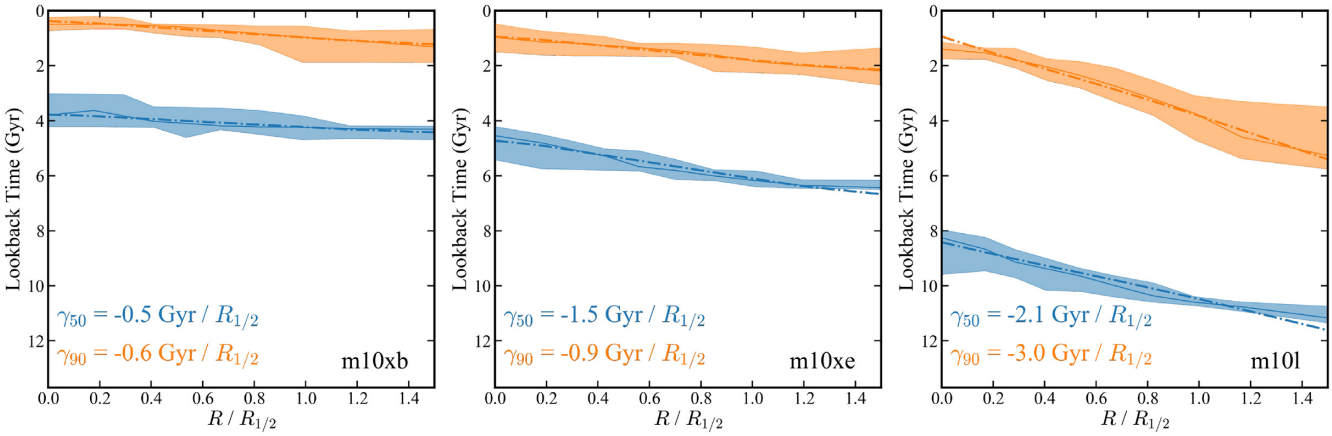

Figure 3. Age versus projected radius for three example galaxies – m10xb, m10xe, and m10l from left to right, respectively. These are the same galaxies illustrated in Fig. 2. The times shown are specifically the lookback times to 50 per cent star formation (t_{50}, blue) and the lookback times to 90 per cent star formation (t_{90}, orange). The solid line represents the median age measured at each projected radius for 100 random viewing angles for each galaxy, while the shaded bands show the 99th percentile range in measured age at a given projected radius over all 100 random viewing angles. The corresponding slope of the gradient as defined in equation (1) is shown in the lower left of each panel.

those at the centre of the galaxy in Gyr. We measure the slope of the gradient in two different ways. First, we take the difference between t_{50} and t_{90} in the innermost and outermost bins, and then divide it by the difference in the mean radius of the inner and outer bins. To double check this, we also measure the slope by calculating the least squares fit to a line, and taking the slope of that line. We find that the different methods of measuring the slope make little difference, and the variation in gradient over projection angle is a much larger effect. Furthermore, if we measure the age gradients in 3D instead of in projection, the gradients tend to be steeper, this is simply due to the fact that if a galaxy is viewed in projection, the younger stars in the centre are mixed with older stars in the outskirts, that appear in the centre in projection.

The median values for the gradients we measure for each galaxy in our simulated sample are listed in Table 1. We see that most of the dwarf galaxies show a clear negative age gradient, where the stars are younger in the inner regions and older in the outskirts. Some of the gradients are small, or consistent with being flat, but most are clearly negative. The gradients are measured by dividing the stellar distribution along the chosen projection into 10 radial bins within 1.5 × $R_{1/2}$, such that there are an equal number of star particles in each bin. All galaxies have >80 star particles per bin, or >800 star particles within 1.5 × $R_{1/2}$, however the results do not vary significantly with bin choice. The slope of the gradient is then measured by fitting a line to the gradient and measuring the slope. The fit is restricted to 1.0 × $R_{1/2}$ in order for the slope to have the form seen in equation (1). Interestingly, the value of the gradient does not appear to correlate with standard parameters such as halo mass, stellar mass, or V_{max} (see appendix). However, there is a correlation with galaxy age.

Fig. 4 shows the relationship between a galaxy's age gradient and the overall age of the galaxy. The error bars on the gradient values are calculated by taking 100 random projections through the galaxy, calculating the age gradient for that projection, and then measuring the slope of the age gradient for every projection. The error bars reflect the minimum and maximum of slope of the age gradient over all projections for each galaxy. We see that earlier forming galaxies show more significant (more negative) age gradients, while later forming galaxies have smaller (less negative) age gradients. We discuss the origin of this trend in Section 4 and conclude that it is driven by a combination of mergers and the strong stellar feedback inherent in our simulations.

4 DISCUSSION

4.1 Origin of age gradients

The standard picture for how stars are distributed in galaxies as a function of age is rooted in the 'inside-out' model, where star formation is first confined to the centre of the galaxy and proceeds in the outer reaches only at later times (Larson 1976; Mo, Mao & White 1998; Avila-Reese & Firmani 2000; Brook et al. 2006; Pilkington et al. 2012; Aumer & White 2013). Such a distribution is seen observationally in larger galaxies including disc galaxies (Gil de Paz et al. 2005, 2007; Martin et al. 2005; Nelson et al. 2012, 2016) and ellipticals (van Dokkum et al. 2010; Patel et al. 2013). Based on how age gradients are measured in this work, inside-out formation would correspond to a positive value of γ_{50} and γ_{90}. From Fig. 4 we see that essentially none of the dwarf galaxies studied in this work show positive age gradients in a striking difference from that naive expectation.

Unlike large discs and elliptical galaxies, dwarfs are much less ordered, and this likely contributes to the lack of the characteristic inside-out age gradients. Two possible mechanisms for inverting age gradients are mergers, which could bring in stars and modify an existing gradient, and stellar feedback, which could heat stars progressively over time, pushing older stars to the outskirts.

Both galaxy mergers and mergers with dark matter haloes containing no stars could drive SFH gradients. Specifically, mergers (either with stars or without) can heat the pre-existing stellar distribution (Starkenburg & Helmi 2015; Benitez-Llambay et al. 2016; Leaman et al. 2017). Since these mergers tend to happen at early times, they might be responsible for driving the spread with formation time as they would be more likely to heat older stars.

Mergers with galaxies that contain stars can also drive age gradients by preferentially adding stars to the outskirts of a galaxy. This is similar to how the stellar halo of Milky Way-size galaxies is believed to be built (Bullock & Johnston 2005; Cooper et al.

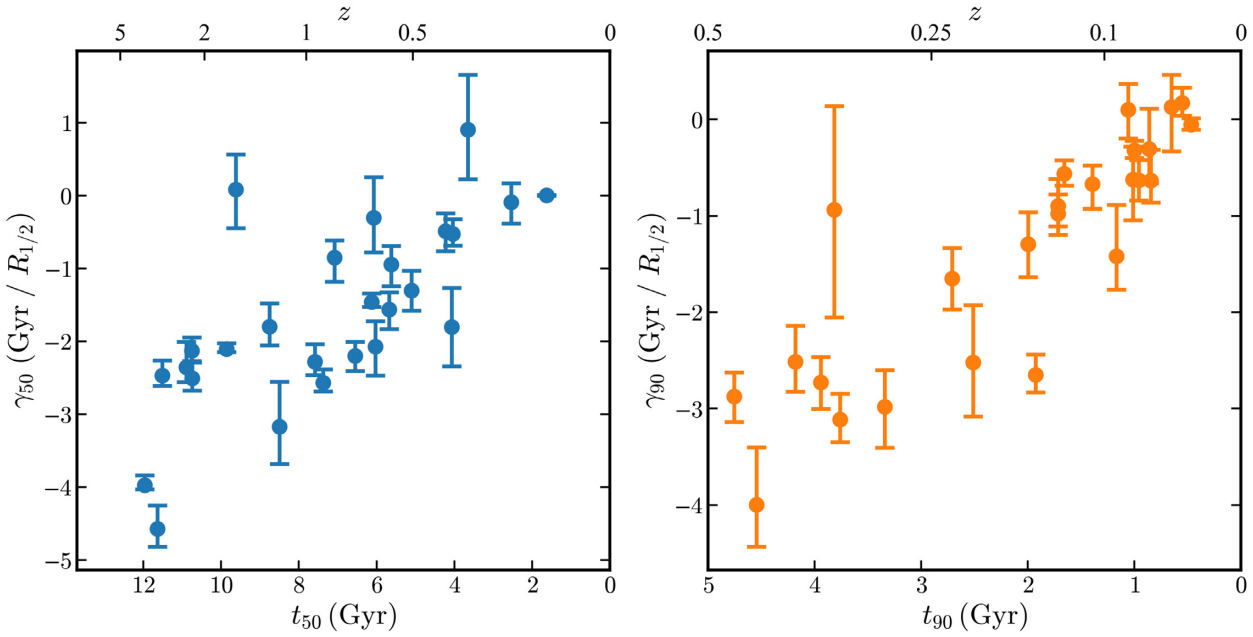

Figure 4. Age gradients as defined in equation (1) for all of the galaxies in the sample, plotted against the t_{50} (median age of stars, left) or t_{90} (age of the youngest 10 per cent of stars, right) of all the stars in the galaxy. Error bars represent the variation over all projections. There is a clear trend with star formation time, such that galaxies that form earlier tend to have stronger gradients.

2010). Since most mergers are with lower mass objects, most accretion events among dwarfs galaxies likely include many ultrafaint dwarf galaxies with very old stellar populations. Mergers of this kind could deposit old stars to the outskirts of the primary dwarfs.

In reality, galaxies experience both mergers and feedback. Therefore, the exact origin of a gradient in a galaxy must be evaluated on a case-by-case basis. However, some broad conclusions can be drawn from analysis of this suite of simulations. Merger history can play some part in the formation of an age gradient, however, the galaxies in our sample generally do not have many accreted stars. This is shown in Table 1 where we list the fraction of stars that were brought in via mergers. In general, the fraction of accreted stars is very low <5 per cent. However, when the fraction of accreted stars is high, it can have an impact on gradient formation by both creating and destroying an age gradient. For example, several galaxies with flatter age gradients (such as m10xd, m10xd_A, and m10xh) have late-time mergers with another galaxy. If the merging galaxy has a sufficiently extended SFH, than the merger adds young stars to the outskirts and prevents an age gradient from forming. In particular, m10xh has a late-time merger with a galaxy that has a late SFH and thus the stars added to the outskirts are actually younger on average than the stars from the main galaxy creating a positive age gradient. In contrast, some galaxies like m10xi have strong age gradients that form due to mergers. In the specific case of m10xi, it has a merger with several small objects at $z \simeq 1$, which bring in almost exclusively ancient stars and rapidly build an age gradient. The relationship between strength of the gradient and the specifics of mergers naturally explains the trend between strength of the age gradient and formation time. Objects that have mergers that bring in young stars at late times would have both late formation times and flat age gradients. While objects that have earlier mergers that bring in ancient stars would have earlier formation times and strong age gradients.

Interestingly, while most of the galaxies in our sample have little accreted stars, they still can have pronounced age gradients. Evidence of this can be seen in Figs 5 and 6. Fig. 5 shows the migration of star particles from their position where they formed ($r_{\rm birth}$) to where they end up at $z = 0$, with the points coloured by the age of the star particle for the same systems shown in Figs 2 and 3. Every system regardless of strength of the age gradient has a population of old stars that migrate outwards after they form, these star particles lie above the one-to-one line, denoted by the black dashed line in the figure. Whether or not a galaxy has a strong age gradient depends on what happens at late times. For galaxies with weak age gradients (such as m10xb) there is a large population of young stars that form along the one-to-one line that extends out to large radii up to, and including the radius at which the older stellar population has migrated out to. In contrast, the galaxies in Fig. 5 that have stronger gradients (m10xe and m10l) have younger star formation that is restricted to smaller radii.

This is further emphasized by Fig. 6 which shows the half-mass radii of all of the systems over time, normalized to the $z = 0$ value. The sample is subdivided in two, gradients steeper than the median ($\gamma_{90} < -1.4$) and gradients flatter than the median. The solid line represents the median of both samples and the shaded region contains 68 per cent of the data. When the sample is divided in this way there is a clear difference between galaxies with strong gradients, and those with weaker ones. Galaxies with strong age gradients tend to establish their sizes at early times. Thus, late-time star formation occurs at roughly the same extent that older star formation did. However, the older stars have been subsequently heated out to larger radii, creating a strong gradient. In contrast, galaxies with weak gradients are increasing in size at all times. Thus, the young stars form at radii comparable to, or larger than the radii out to which older stars have been heated, creating a flatter age gradient. This also explains the trend with overall stellar age, as galaxies with older stellar distributions established their

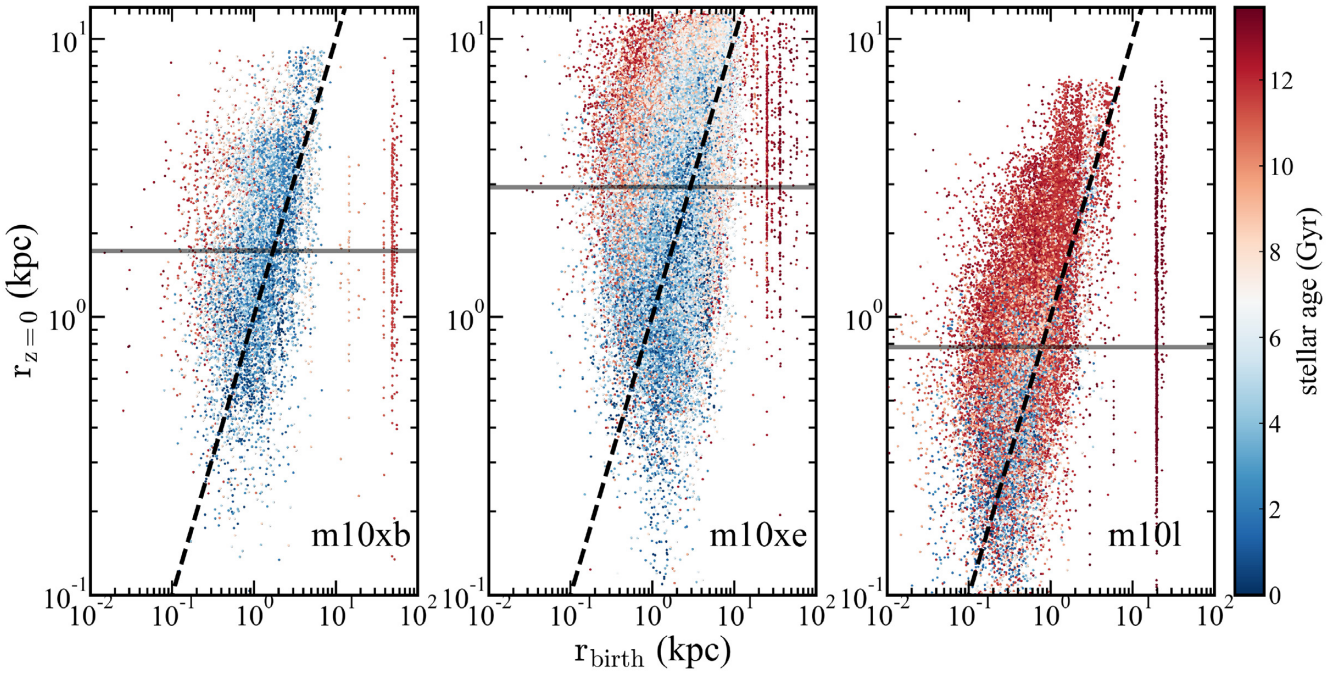

Figure 5. The distance of the star particle from the centre of the halo at birth (r_{birth}) versus the distance of the star from the centre at $z = 0$ ($r_{z=0}$), with the points coloured by the overall age of the star, for the same three simulated haloes as in Figs 2 and 3. The black dashed line shows the one-to-one line, stars above that line have moved outwards since birth, and stars below have moved inwards. the gray horizontal line is the half-mass radius for each system. Older stars in every system always lie above the one-to-one line showing that a majority of stars at large radii today were born closer to the centre of the halo and heated outwards. Younger stars tend to be born along the one-to-one line, with some scatter due to the star particle's orbit. The extent to which a galaxy has an age gradient is determined by how extended this young star formation is. For example, in m10xb the late-time star formation is very extended resulting in a minimal age gradient. However, in m10l young star formation is restricted to the inner regions resulting in a large gradient. Most of the systems also have an obvious contribution of old stars from mergers, which show up as vertical lines at large radii. However, these are few in number compared to stars that form inside the main galaxy. The accreted stars also tend to mix evenly through the extent of the system, and do not contribute to gradient formation in most cases.

masses and sizes at earlier times, whereas galaxies with later star formation are constantly growing in both stellar mass and galaxy size.

Also notable in Fig. 5 is the impact of mergers can be clearly seen. In all three panels, the galaxies have a contribution of stars that were born well outside of the galaxy, which appear as vertical streaks of points. In all three of these systems, the stars are old. However, in all cases the number of stars brought in by these mergers is negligible compared to the number of stars that form inside the galaxy. In addition, the stars from mergers tend to distribute themselves throughout the galaxy instead of preferentially ending up in the outskirts, and thus do not contribute much to the formation of an age gradient.

One obvious physical mechanism for creating this heating is stellar feedback processes similar to those that are responsible for creating cores in dwarf galaxies (Pontzen & Governato 2012; Di Cintio et al. 2014; Chan et al. 2015; Oñorbe et al. 2015; Dutton et al. 2016; Read et al. 2016; Fitts et al. 2017). Stellar feedback from supernovae can quickly expel gas from a dwarf galaxy. The resultant change in the gravitational potential can perturb the orbits of dark matter particles and create cored dark matter halo profiles. A similar process could reorder the stars in the galaxy. One obvious indication that this is happening would be if the strength of the age gradient correlates in some way with the formation of a core in the dark matter halo.

As seen in previous works involving dwarf galaxies in FIRE (Chan et al. 2015; Oñorbe et al. 2015; El-Badry et al. 2016; Fitts et al. 2017) the dark matter haloes of dwarf galaxies in our sample can be strongly affected by stellar feedback, with cores getting larger as the stellar mass increases, up to the limit of our sample. Naturally, if stellar feedback were responsible for creating age gradients as well as cores, a first-order test would be to see if the strength of the gradient correlates with the size of the core. To measure core strength we ran dark matter only versions of our simulations and have compared the densities near the centre both with and without hydrodynamics. In Fig. 7, we plot the same data as Fig. 4, but now colour the points by the ratio of the dark matter density in the full hydrodynamics simulation to that of the corresponding dark matter only simulation (ρ_{hydro}/ρ_{dmo}) measured at 500 pc. The left-hand panels in Fig. 7 show this for all galaxies in our sample and there appears to be no relation between core formation and age gradient. However, this sample includes galaxies with late-time mergers, which could flatten out the age gradient, but may have a different impact on the core. Furthermore, some of the smaller galaxies in our sample do not have enough stars for feedback to have affected the core (e.g. Fitts et al. 2017). Both of these mechanisms would act to wash out any obvious relation between core formation and gradient formation.

In the right-hand panel of Fig. 7 we plot the same relation, but only for galaxies that have enough stellar mass to form a core ($M_{star} > 5 \times 10^6$ M$_\odot$), and have few accreted stars ($f_{acc} \leq 5$ per cent). For these galaxies, we see some indication that galaxies with larger cores have flatter age gradients. This trend can be understood in tandem with the relationship between gradient strength and formation time.

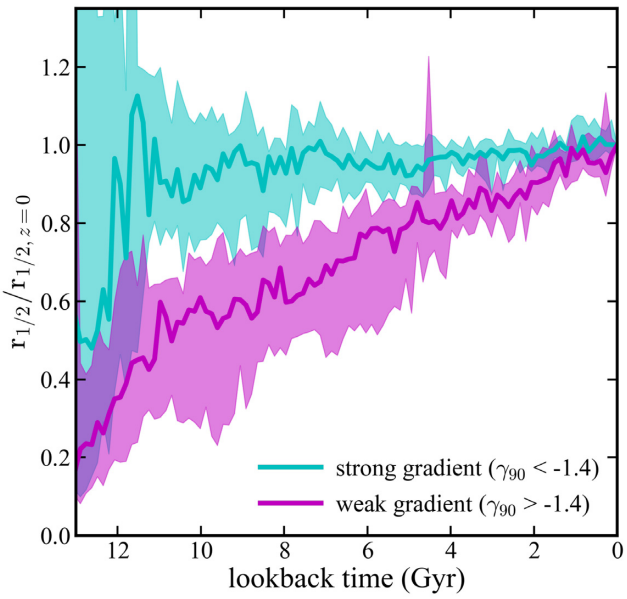

Figure 6. The ratio between the 3D half-mass radius ($r_{1/2}$), and present-day half-mass radius ($r_{1/2,\,z=0}$) as a function of time. The sample is divided into galaxies with strong age gradients ($\gamma_{90} < -1.4$) and weak gradients ($\gamma_{90} > -1.4$), where -1.4 is the average value of γ_{90}. Galaxies with stronger gradients tend to establish their sizes at early times, thus as stars are heated, they are heated beyond the radius where stars are actively forming resulting in a large age gradient. Galaxies with weaker gradients tend to be growing even at late times resulting in young star formation in the outskirts of the galaxy. While only γ_{90} is shown the results do not change if $\gamma 50$ is used instead.

Early-forming galaxies have more feedback at early times to push out stars. Subsequent star formation deposits young stars at small radius (as seen in Fig. 6) creating a strong age gradient. However, any core in the dark matter halo that formed along with this early star formation can get rebuilt from subsequent dark-matter mergers, an effect that has been seen in previous FIRE simulations (Oñorbe et al. 2015). Subsequent star formation was not enough to drive the creation of a core, nor to drive younger stars out, but enough to drive the median age of the inner regions to younger ages. For later forming galaxies, large star formation rates at late times created a large core. This late star formation was also more extended in these galaxies, often well beyond the radius out to which older stars are heated, resulting in a galaxy with a flat age gradient. Completely decoupling all these effects would require a much larger sample of galaxies with a variety of accretion histories at fixed stellar mass. Investigations of this nature with a larger sample of dwarf galaxies could help to decouple the time-scales of core formation, gradient formation, and mergers from galaxies.

As a final caveat, several recent works have investigated the connection between core formation in dwarf galaxies and the density threshold of star formation implemented in cosmological simulations of galaxy formation (Benitez-Llambay et al. 2018; Bose et al. 2018; Dutton et al. 2018). In general, it appears as though core formation is intimately tied to the density threshold of star formation assumed. If the density threshold is too low ($n \simeq 0.1\,\mathrm{cm}^{-3}$), gas is allowed to turn into stars a low densities compared to the local dark matter density, and cannot dominate the local gravitational potential, preventing the formation of cores. On the other hand, if the density threshold is high ($n \simeq 10$–$100\,\mathrm{cm}^{-3}$), the gas can dominate the local gravitational potential. The density threshold for star formation used in our FIRE-2 simulations is $n = 1000\,\mathrm{cm}^{-3}$, which is well into the regime where star formation is able to induce core formation. The relation between star formation threshold and core formation complicates the picture of how star formation impacts galaxy evolution. If the formation of age gradients is tied to feedback, then it could also be similarly affected by the threshold of star formation. If so, then observational explorations of age gradients in dwarf galaxies may provide an interesting direct constraint on galaxy formation simulations and help define realistic star formation thresholds.

4.2 Observed dwarf galaxies

It has long been known that the classical dwarf satellites of the Milky Way and galaxies throughout the Local Volume show metallicity gradients (Harbeck et al. 2001; Battaglia et al. 2006; Bernard et al. 2008; McConnachie 2012; Martínez-Vázquez et al. 2015; Kacharov et al. 2017; Okamoto et al. 2017). However, to date, observations of the distribution of stellar ages as a function of radius, are rare, particularly at this mass scale, making a direct comparison difficult.

One comparison we can make is to the data presented in Hidalgo et al. (2013), who observed four nearby dwarf galaxies (Cetus, Tucana, LGS 3, and Phoenix) and measured the SFHs of these galaxies in radial bins. The results once again qualitatively agree with our results. LGS 3 and Phoenix show a fairly strong spread in SFH where the age of the latest forming stars increases with increasing radius. Tucana shows a smaller spread in its SFH, and Cetus has no detectable spread. It is difficult to use this data to quantify whether or not the formation time is correlated to the spread in the SFH because many of these galaxies are not isolated, and are therefore may be quenched by environmental effects (Fillingham et al. 2018). Indeed, the galaxies with smallest gradients in the Hidalgo et al. (2013) sample (Cetus and Tucana) are older; however, both of these galaxies are quenched whereas all the isolated dwarf galaxies in FIRE studied in this paper are actively star forming. Another comparison that can be made is to various integral field unit surveys of galaxies that have become common over the past several years. Because these surveys provide spectral coverage over each pixel, it is possible to measure SFH variation over the face of a galaxy.

García-Benito et al. (2017) measured the spatially resolved SFHs for 661 galaxies within the CALIFA survey. The stellar mass range of their targeted galaxies is $10^{8.4}$–10^{12} $\mathrm{M}_{\odot}$, and thus only the most massive of the galaxies in our sample are directly comparable to the results from the CALIFA survey. However, there are some interesting trends that are hinted at in García-Benito et al. (2017). In general, they find that their galaxies show age gradients with older stars in the central regions, and younger stars at the outskirts consistent with typical inside-out galaxy formation. These massive galaxies also show very weak gradients in their SFHs. Interestingly, this gradient actually strengthens in the lowest mass bin in their sample, $M_{\mathrm{star}} = 10^{8.4}$–$10^{9.9}$ $\mathrm{M}_{\odot}$. In this bin, the stars are in general later forming, but the gradient between the inner and outermost regions is larger. This could potentially point towards some interesting evolution between the most massive galaxies in our sample which show slightly negative or flat gradients, and the lowest mass galaxies in the CALIFA sample, which show large positive age gradients. Additionally, it is possible that there is a strong difference between SFHs measured from spectra, and those measured from CMDs. Such

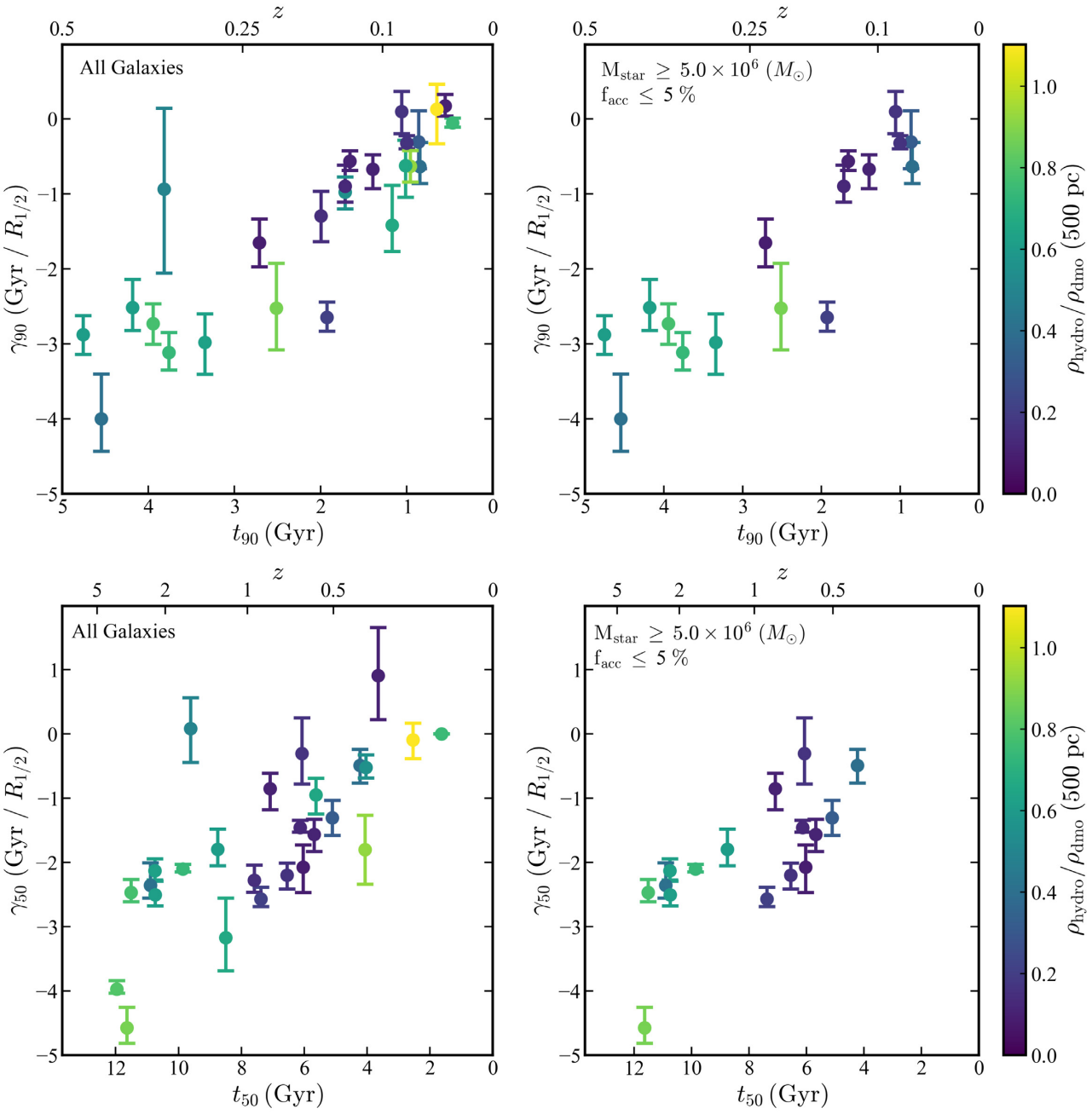

Figure 7. Strength of the age gradient as a function of formation time. The left two panels are identical to Fig. 4, however the points are now coloured by the density ratio between the full hydrodynamics run and the corresponding halo from a dark matter only simulation. For a scenario where feedback is the only cause of the age gradients, one would expect a correlation between core formation and strength of gradient. However, galaxies with too low of a stellar mass to form a core, and galaxies with many stars brought in by mergers could contaminate this relationship. The right-hand panels attempt to remove these contaminants, by removing any galaxy with less than 5×10^6 $M_\odot$ in stellar mass, and with greater than 5 per cent accreted stars. Once these are removed there appears to be a slight relation between core formation and strength of the gradient, where objects flat gradients tend to have recent star formation, and large cores. This potentially points towards these stellar populations being more well mixed due to recent star bursts driving feedback and both creating cores, and smoothing out an age gradient.

a difference was pointed out by Leitner (2012), who compared SFH measured with both SDSS spectra and CMDs and found a that they disagree, with SFHs from CMDs implying a much slower growth. Currently, while there are many dwarf galaxies throughout the Local Volume with CMD-measured SFHs, even some with multiple fields per galaxy, they represent a very non-uniform sample. This is because most of the galaxies have been observed to different depths and at different locations throughout the extent of the galaxy. Some systems suffer from crowding effects, or poorly constrained SFHs due to the relatively shallow depth of the measured CMDs. An analysis of CMD-based SFHs taking into account the non-uniformity and incompleteness of the observed

sample, and how it compares to the results presented in this paper is currently underway, first results of which can be found in Albers et al. (2019).

4.3 Implications for SFH measurements

If real dwarf galaxies have SFH gradients similar to those predicted in our simulations, it could impact the interpretation of current measurements of SFHs and plans for future measurements. This is because CMD-derived SFHs often rely on photometric observations via space-based facilities, such as the *Hubble Space Telescope* (*HST*), with fields of view that cover only 10 per cent (or less) of the area of nearby galaxies. If the galaxy has a strong age gradient, the placement of the field with respect to the galaxy's centre could lead to a biased view of the overall global SFH of the galaxy.

Here, we explore the potential bias that could arise from fractional spatial coverage by measuring the spread in SFHs as a function of projected radius. Of course any bias in the recovered SFH depends on several factors including the survey field's distance from the centre of the galaxy, the size of the field of view with respect to the galaxy, and the steepness of the gradient. Observationally, the first two are known, but the strength of the gradient cannot be determined without first measuring the SFH. Our goal is to estimate the nature and magnitude of the effect using mock observations of our galaxy sample.

Fig. 8 shows the result of this exercise. We have computed the values of t_{50} and t_{90} for all galaxies in our sample, each viewed from 100 different random angles. We then measured the spread in SFH in discrete bins of width 0.1 $R_{1/2}$. The figure shows the measured ages relative to the true value of t_{50} or t_{90} for all of the stars within 10 per cent of the virial radius of the galaxy's dark matter halo. The solid lines in Fig. 8 show the median of the error in age as a function of projected radius. The shaded regions with the darker and lighter bands show the 68 per cent and 95 per cent distributions in deviation from the true age of the galaxy.

The bias in the SFH measured at different points throughout the galaxy works in the direction one would expect: the inner regions of the galaxy are biased younger than the global SFH of the galaxy, and the outskirts are biased older than the global value. Interestingly, the SFH measured around the projected half-mass radius matches well to the galaxy-averaged value, with a relatively small scatter. We can apply this information to current observed SFHs such as those in Weisz et al. (2014a). In general, this data is archival *HST* data, where the fields were selected to maximize the number of stars. Therefore, the fields tend to be near the centres of galaxies, and are almost always within the half-light radius. Assuming the half-mass and half-light radii are comparable in size, this would imply that many CMD-based SFHs in Weisz et al. (2014a) are biased young relative to the global SFH of the galaxy as mentioned in section 4.1 of Weisz et al. (2014a). This motivates additional observations of these galaxies outside of the half-light radii.

4.4 Implications for future observations

As discussed in Section 4.3, age gradients can potentially bias SFHs inferred from CMD studies that cover only a fraction of a dwarf galaxy. This result may have important implications for planning future observing campaigns to infer galaxy SFHs with resolved stellar populations. Without a careful accounting for the age gradient, significant errors in the SFH can result. Where fields should be placed within galaxies in order to recover the correct SFH will become even more important in the future for the *James Webb Space Telescope* (*JWST*), which has a similar field of view as *HST* but will be able to measure SFHs for many more galaxies throughout the Local Volume. Our results shown in Fig. 8 suggest that fields at radii close to $R_{1/2}$ are optimal. However, for galaxies of these sizes beyond about 1.3 Mpc the entire galaxy should fall within one *HST* or *JWST* pointing, thus eliminating the need to aim for $R_{1/2}$. Note that we find no significant spatial or angular variation at fixed projected radius – it is the distance from the galaxy centre that matters most.

Even further on the in the future, after *JWST*, *WFIRST* will be able to cover most of the area of galaxies throughout the Local Volume; however, crowding effects could limit its ability to measure accurate SFHs for the inner regions of these galaxies. If crowding affects the ability to do stellar population studies within $R_{1/2}$, then measured SFHs could be biased old with respect to the global stellar distribution.

One potential caveat of the analysis in this section concerns whether the simulated galaxies we study here are representative of dwarf galaxies in the Local Group. The relative isolation of the galaxies in our sample could make their SFHs differ from dwarf galaxies in the vicinity of a larger galaxy. One place where our sample is truly not representative is to the satellites of the MW and M31, where most low-mass galaxies are not actively star forming. However, it is possible that host interactions influence dwarf galaxy evolution even beyond the virial radii of M31 or the MW. Garrison-Kimmel et al. (2019) looked at this question by comparing dwarf galaxies simulated with FIRE physics. They concluded that the isolated dwarfs used in this work form significantly later than satellite galaxies at all masses. Interestingly, they also form slightly later on average than galaxies that are beyond the virial radius of a larger system but within about 1 Mpc of a Local Group host. However, this difference is not statistically significant for galaxies of a stellar mass above 10^6 $M_\odot$, which all but two of the galaxies used in this sample are.

5 CONCLUSION

In this work, we have studied the presence of SFH gradients in FIRE-2 simulations of dwarf galaxies. Almost all of our galaxies, which have stellar masses between $10^{5.5}$ and $10^{8.6}$ $M_\odot$, show gradients in their SFHs with younger stars at the centre and older stars at the outskirts. The slope of the gradients varies widely between galaxies, and does not seem to show a strong correlation with stellar mass and halo mass. However, as shown in Fig. 4, there is a clear correlation between the slope of the age gradient and the overall age of the galaxy.

The origin of these age gradients is a complicated mixture of both mergers and stellar feedback. Mergers can both create and destroy age gradients based on the timing of a merger, and the SFH of the merging system. However, few systems have a large number of accreted stars. Stellar feedback produces potential fluctuations that heat stars and also launches molecular outflows that subsequently form stars (El-Badry et al. 2016). Earlier forming galaxies have had a longer time for their stars to be dynamically heated by multiple feedback episodes changing the gravitational potential of the galaxy via the removal of gas. Early feedback events also produce more outflowing, star-forming gas, which eventually deposits older stars at larger radii. This heating of stars is seen in nearly all the galaxies in our suite of simulations (see Fig. 5).

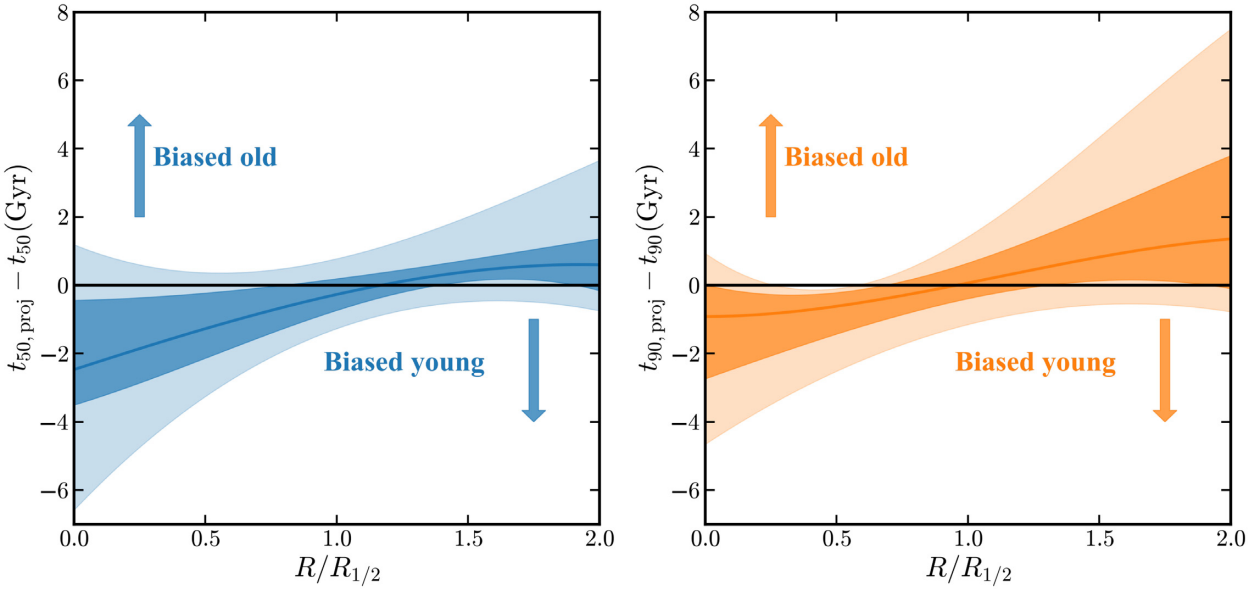

Figure 8. Bias in inferred SFH that would occur from studying a stellar population at a given projected radius in units of a galaxy's half-mass radius. The offset in true t_{50} (median age) and t_{90} (90 percentile youngest stars) are shown in the left-hand and right-hand panels, respectively. The solid lines represent the median bias in age determined by 'stacking' all of our galaxies and observing them over 100 viewing angles each. The darker and lighter shaded regions represent the 68 per cent and 95 per cent contours of the distributions. The 'pinch' at a time-bias of zero at $R/R_{1/2} \simeq 1$ in both panels shows that photometric fields positioned near a galaxy's half-light radius are optimal for single-pointing stellar population studies aimed at providing an unbiased view of a galaxy's global SFH.

The formation of an age gradient is determined by the subsequent evolution of the galaxy. Galaxies with strong gradients tend to establish their sizes at early times, thus the extent of young star formation is smaller than the extent to which older stars have been heated outwards by stellar feedback. On the other hand, galaxies with weaker age gradients tend to be growing steadily throughout cosmic time, resulting in young star formation that extends to or beyond the radius out to which stars have been heated. Furthermore, we see a trend between strength of the age gradient and core formation in the dark matter halo. Systems with flat age gradients tend to have large dark matter cores, as these systems have had more recent intense star formation which builds a core. For galaxies with strong age gradients, these systems tend to have stronger star formation at earlier times, and over time these stars were heated by stellar feedback. At late times the SFR was low enough that feedback could not drive a core in the dark matter halo, or eject stars into the outskirts of the galaxy, but was enough to drive the median age of the central regions to younger ages.

Observational comparisons to available data are difficult; however, there are some broad consistencies. First, dwarf galaxies are known to have median age gradients with younger stars at the centre and older stars at the outskirts. Resolved SFH work such as that from Hidalgo et al. (2013) supports the existence of SFH gradients, but provides weak evidence of a trend with formation time.

The existence of significant age gradients in dwarf galaxies could potentially lead to observational biases in stellar population studies that are restricted to a limited area of a dwarf. Fig. 8 shows that inner fields are biased young and outer fields are biased old relative to the global SFH of the galaxy. The ideal location for a photometric field to provide an unbiased measure of the global SFH is near the 2D half-light radius.

The observation of SFH gradients in dwarf galaxies has several implications for the future of galaxy formation studies. If dwarf galaxies in the Local Volume show a gradient in their SFHs, measuring how this gradient scales with formation time could be useful in calibrating feedback models. However, accurate calibration of feedback models would require resolved SFHs for many dwarf galaxies at several radii in order to accurately measure the slopes of the gradient.

Importantly, the spread in SFH with radius is large enough that SFHs derived from single-field CMDs may not be accurate. The SFH can vary significantly with radius, potentially biasing results from small fields by several Gyrs. Thus, truly understanding the formation of dwarf galaxies will require observations covering large areas of the galaxy, or at least some correction for how incomplete coverage can bias measurements of the SFH. If only a single pointing is possible then Fig. 8 suggests that the field should be centred near $R_{1/2}$. Such considerations should be taken into account as we move towards stellar population studies in the era of *JWST*, *WFIRST*, and 30m-class telescopes.

ACKNOWLEDGEMENTS

We thank the anonymous referee for their insightful comments on the draft. ASG and JSB were supported by NSF AST-1518291, HST-AR-14282, and HST-AR-13888. ASG is further supported by the McDonald Observatory at the University of Texas at Austin, through the Harlan J. Smith fellowship. MBK and AF acknowledge support from NSF grant AST-1517226. MBK also acknowledges support from NSF CAREER grant AST-1752913 and from NASA grants NNX17AG29G and HST-AR-13888, HST-AR-13896, HST-AR-14282, HST-AR-14554, HST-AR-15006, HST-GO-12914, and HST-GO-14191 from the Space Telescope Science Institute, which is operated by AURA, Inc., under NASA contract

NAS5-26555. MCC was supported by NSF AST-1815475. DRW is supported by a fellowship from the Alfred P. Sloan Foundation. He also acknowledges support from the Alexander von Humboldt Foundation and from HST-GO-13768, HST-GO-15476, HST-AR-13888, HST-AR-13925, HST-AR-15006, and JWST-ERS-01334. AW was supported by NASA through ATP grant 80NSSC18K1097 and grants HST-GO-14734 and HST-AR-15057 from STScI. RF acknowledges support from the Swiss National Science Foundation (grant no. 157591). CAFG was supported by NSF through grants AST-1517491, AST-1715216, and CAREER award AST-1652522, by NASA through grants NNX15AB22G and 17-ATP17-0067, and by a Cottrell Scholar Award from the Research Corporation for Science Advancement. This work used computational resources of the University of Texas at Austin and the Texas Advanced Computing Center (TACC; http://www.tacc.utexas.edu), the NASA Advanced Supercomputing (NAS) Division and the NASA Center for Climate Simulation (NCCS), and the Extreme Science and Engineering Discovery Environment (XSEDE), which is supported by National Science Foundation grant number OCI-1053575.

REFERENCES

Albers S. M. et al. 2019, preprint (arXiv:1902.04040)
Aumer M., White S. D. M., 2013, MNRAS, 428, 1055
Avila-Reese V., Firmani C., 2000, Rev. Mex. Astron. Astrofis., 36, 23
Battaglia G. et al., 2006, A&A, 459, 423
Beccari G. et al., 2014, A&A, 570, A78
Behroozi P. S., Wechsler R. H., Wu H.-Y., 2013a, ApJ, 762, 109
Behroozi P. S., Wechsler R. H., Wu H.-Y., Busha M. T., Klypin A. A., Primack J. R., 2013b, ApJ, 763, 18
Benitez-Llambay A., Navarro J. F., Abadi M. G., Gottlöber S., Yepes G., Hoffman Y., Steinmetz M., 2016, MNRAS, 456, 1185
Benitez-Llambay A., Frenk C. S., Ludlow A. D., Navarro J. F., 2018, MNRAS, 488, 2387
Bernard E. J. et al., 2008, ApJ, 678, L21
Bose S., et al., 2018, MNRAS, 486, 4790
Boylan-Kolchin M., Bullock J. S., Kaplinghat M., 2011, MNRAS, 415, L40
Boylan-Kolchin M., Bullock J. S., Garrison-Kimmel S., 2014, MNRAS, 443, L44
Boylan-Kolchin M., Weisz D. R., Johnson B. D., Bullock J. S., Conroy C., Fitts A., 2015, MNRAS, 453, 1503
Brook C. B., Kawata D., Martel H., Gibson B. K., Bailin J., 2006, ApJ, 639, 126
Brown T. M. et al., 2014, ApJ, 796, 91
Bullock J. S., Boylan-Kolchin M., 2017, ARA&A, 55, 343
Bullock J. S., Johnston K. V., 2005, ApJ, 635, 931
Bullock J. S., Kravtsov A. V., Weinberg D. H., 2000, ApJ, 539, 517
Chan T. K., Kereš D., Oñorbe J., Hopkins P. F., Muratov A. L., Faucher-Giguère C. A., Quataert E., 2015, MNRAS, 454, 2981
Chan T. K., Kereš D., Wetzel A., Hopkins P. F., Faucher-Giguère C. A., El-Badry K., Garrison-Kimmel S., Boylan-Kolchin M., 2018, MNRAS, 478, 906
Cicuéndez L., Battaglia G., 2018, MNRAS, 480, 251
Cicuéndez L. et al., 2018, A&A, 609, A53
Cole A. A., Weisz D. R., Dolphin A. E., Skillman E. D., McConnachie A. W., Brooks A. M., Leaman R., 2014, ApJ, 795, 54
Collins M. L. M. et al., 2013, ApJ, 768, 172
Cook K. H., Mateo M., Olszewski E. W., Vogt S. S., Stubbs C., Diercks A., 1999, PASP, 111, 306
Cooper A. P. et al., 2010, MNRAS, 406, 744
del Pino A., Aparicio A., Hidalgo S. L., 2015, MNRAS, 454, 3996
Di Cintio A., Brook C. B., Macciò A. V., Stinson G. S., Knebe A., Dutton A. A., Wadsley J., 2014, MNRAS, 437, 415
Dolphin A. E., 2002, MNRAS, 332, 91
Dutton A. A., Macciò A. V., Frings J., Wang L., Stinson G. S., Penzo C., Kang X., 2016, MNRAS, 457, L74
Dutton A. A., Macciò A. V., Buck T., Dixon K. L., Blank M., Obreja A., 2018, MNRAS, 486, 655
Efstathiou G., 1992, MNRAS, 256, 43P
El-Badry K., Wetzel A., Geha M., Hopkins P. F., Kereš D., Chan T. K., Faucher-Giguère C.-A., 2016, ApJ, 820, 131
Escala I. et al., 2018, MNRAS, 474, 2194
Faria D., Feltzing S., Lundström I., Gilmore G., Wahlgren G. M., Ardeberg A., Linde P., 2007, A&A, 465, 357
Faucher-Giguère C.-A., Lidz A., Zaldarriaga M., Hernquist L., 2009, ApJ, 703, 1416
Fillingham S. P., Cooper M. C., Wheeler C., Garrison-Kimmel S., Boylan-Kolchin M., Bullock J. S., 2015, MNRAS, 454, 2039
Fillingham S. P., Cooper M. C., Pace A. B., Boylan-Kolchin M., Bullock J. S., Garrison-Kimmel S., Wheeler C., 2016, MNRAS, 463, 1916
Fillingham S. P., Cooper M. C., Boylan-Kolchin M., Bullock J. S., Garrison-Kimmel S., Wheeler C., 2018, MNRAS, 477, 4491
Fitts A. et al., 2017, MNRAS, 471, 3547
Flores R. A., Primack J. R., 1994, ApJ, 427, L1
Fraternali F., Tolstoy E., Irwin M. J., Cole A. A., 2009, A&A, 499, 121
Gallart C. et al., 2015, ApJ, 811, L18
García-Benito R. et al., 2017, A&A, 608, A27
Garrison-Kimmel S. et al., 2017, MNRAS, 471, 1709
Garrison-Kimmel S. et al., 2019, MNRAS, 489, 4574
Geha M., Guhathakurta P., Rich R. M., Cooper M. C., 2006, AJ, 131, 332
Geha M., Blanton M. R., Yan R., Tinker J. L., 2012, ApJ, 757, 85
Gil de Paz A. et al., 2005, ApJ, 627, L29
Gil de Paz A. et al., 2007, ApJ, 661, 115
Graus A. S., Bullock J. S., Boylan-Kolchin M., Weisz D. R., 2016, MNRAS, 456, 477
Hahn O., Abel T., 2011, MNRAS, 415, 2101
Harbeck D. et al., 2001, AJ, 122, 3092
Harris J., Zaritsky D., 2006, AJ, 131, 2514
Hidalgo S. L. et al., 2013, ApJ, 778, 103
Ho N. et al., 2012, ApJ, 758, 124
Hopkins P. F., 2015, MNRAS, 450, 53
Hopkins P. F., 2017, MNRAS, 466, 3387
Hopkins P. F. et al., 2018, MNRAS, 480, 800
Howley K. et al., 2012, preprint (arXiv:1202.2897)
Hunter D. A., Elmegreen B. G., 2006, ApJS, 162, 49
Kacharov N. et al., 2017, MNRAS, 466, 2006
Katz N., White S. D. M., 1993, ApJ, 412, 455
Kirby E. N., Bullock J. S., Boylan-Kolchin M., Kaplinghat M., Cohen J. G., 2014, MNRAS, 439, 1015
Knollmann S. R., Knebe A., 2009, ApJS, 182, 608
Kroupa P., 2001, MNRAS, 322, 231
Krumholz M. R., Gnedin N. Y., 2011, ApJ, 729, 36
Larson R. B., 1976, MNRAS, 176, 31
Leaman R. et al., 2012, ApJ, 750, 33
Leaman R. et al., 2017, MNRAS, 472, 1879
Leitner S. N., 2012, ApJ, 745, 149
Lelli F., McGaugh S. S., Schombert J. M., 2016, ApJ, 816, L14
Makarova L. N., Makarov D. I., Karachentsev I. D., Tully R. B., Rizzi L., 2017, MNRAS, 464, 2281
Martínez-Vázquez C. E. et al., 2015, MNRAS, 454, 1509
Martin D. C. et al., 2005, ApJ, 619, L1
McConnachie A. W., 2012, AJ, 144, 4
McMonigal B. et al., 2014, MNRAS, 444, 3139
McQuinn K. B. W. et al., 2017, ApJ, 834, 78
Monelli M. et al., 2010, ApJ, 722, 1864
Monelli M. et al., 2016, ApJ, 819, 147
Moore B., 1994, Nature, 370, 629
Mo H. J., Mao S., White S. D. M., 1998, MNRAS, 295, 319

Nelson E. J. et al., 2012, ApJ, 747, L28
Nelson E. J. et al., 2016, ApJ, 828, 27
Okamoto S., Arimoto N., Tolstoy E., Jablonka P., Irwin M. J., Komiyama Y., Yamada Y., Onodera M., 2017, MNRAS, 467, 208
Oñorbe J., Garrison-Kimmel S., Maller A. H., Bullock J. S., Rocha M., Hahn O., 2014, MNRAS, 437, 1894
Oñorbe J., Boylan-Kolchin M., Bullock J. S., Hopkins P. F., Kereš D., Faucher-Giguère C.-A., Quataert E., Murray N., 2015, MNRAS, 454, 2092
Patel S. G. et al., 2013, ApJ, 766, 15
Pilkington K. et al., 2012, A&A, 540, A56
Pontzen A., Governato F., 2012, MNRAS, 421, 3464
Read J. I., Agertz O., Collins M. L. M., 2016, MNRAS, 459, 2573
Ricotti M., Gnedin N. Y., 2005, ApJ, 629, 259
Rodriguez Wimberly M. K., Cooper M. C., Fillingham S. P., Boylan-Kolchin M., Bullock J. S., Garrison-Kimmel S., 2018, MNRAS, 483, 4031
Santana F. A. et al., 2016, ApJ, 829, 86
Saviane I., Held E. V., Piotto G., 1996, A&A, 315, 40
Sawala T. et al., 2016, MNRAS, 457, 1931
Simon J. D., Prada F., Vílchez J. M., Blitz L., Robertson B., 2006, ApJ, 649, 709
Skillman E. D. et al., 2017, ApJ, 837, 102
Starkenburg T. K., Helmi A., 2015, A&A, 575, A59
Stinson G. S., Dalcanton J. J., Quinn T., Gogarten S. M., Kaufmann T., Wadsley J., 2009, MNRAS, 395, 1455
Su K.-Y., Hopkins P. F., Hayward C. C., Faucher-Giguère C.-A., Kereš D., Ma X., Robles V. H., 2017, MNRAS, 471, 144
Tollerud E. J. et al., 2012, ApJ, 752, 45
Tolstoy E., Hill V., Tosi M., 2009, ARA&A, 47, 371
van der Marel R. P., Alves D. R., Hardy E., Suntzeff N. B., 2002, AJ, 124, 2639
van Dokkum P. G. et al., 2010, ApJ, 709, 1018
Walmswell J. J., Eldridge J. J., Brewer B. J., Tout C. A., 2013, MNRAS, 435, 2171
Weisz D. R., Dolphin A. E., Skillman E. D., Holtzman J., Gilbert K. M., Dalcanton J. J., Williams B. F., 2014a, ApJ, 789, 147
Weisz D. R., Johnson B. D., Conroy C., 2014b, ApJ, 794, L3
Weisz D. R., Dolphin A. E., Skillman E. D., Holtzman J., Gilbert K. M., Dalcanton J. J., Williams B. F., 2015, ApJ, 804, 136
Wetzel A. R., Tollerud E. J., Weisz D. R., 2015, ApJ, 808, L27
Wheeler C. et al., 2018, preprint (arXiv:1812.02749)
Wolf J., Martinez G. D., Bullock J. S., Kaplinghat M., Geha M., Muñoz R. R., Simon J. D., Avedo F. F., 2010, MNRAS, 406, 1220

APPENDIX A: AGE GRADIENT VERSUS MASS

Fig. A1 shows the relationship between age gradients and halo mass and stellar mass. Unlike the clear trends seen in Fig. 4 between gradient and age, there appears to be no correlation with these other common parameters.

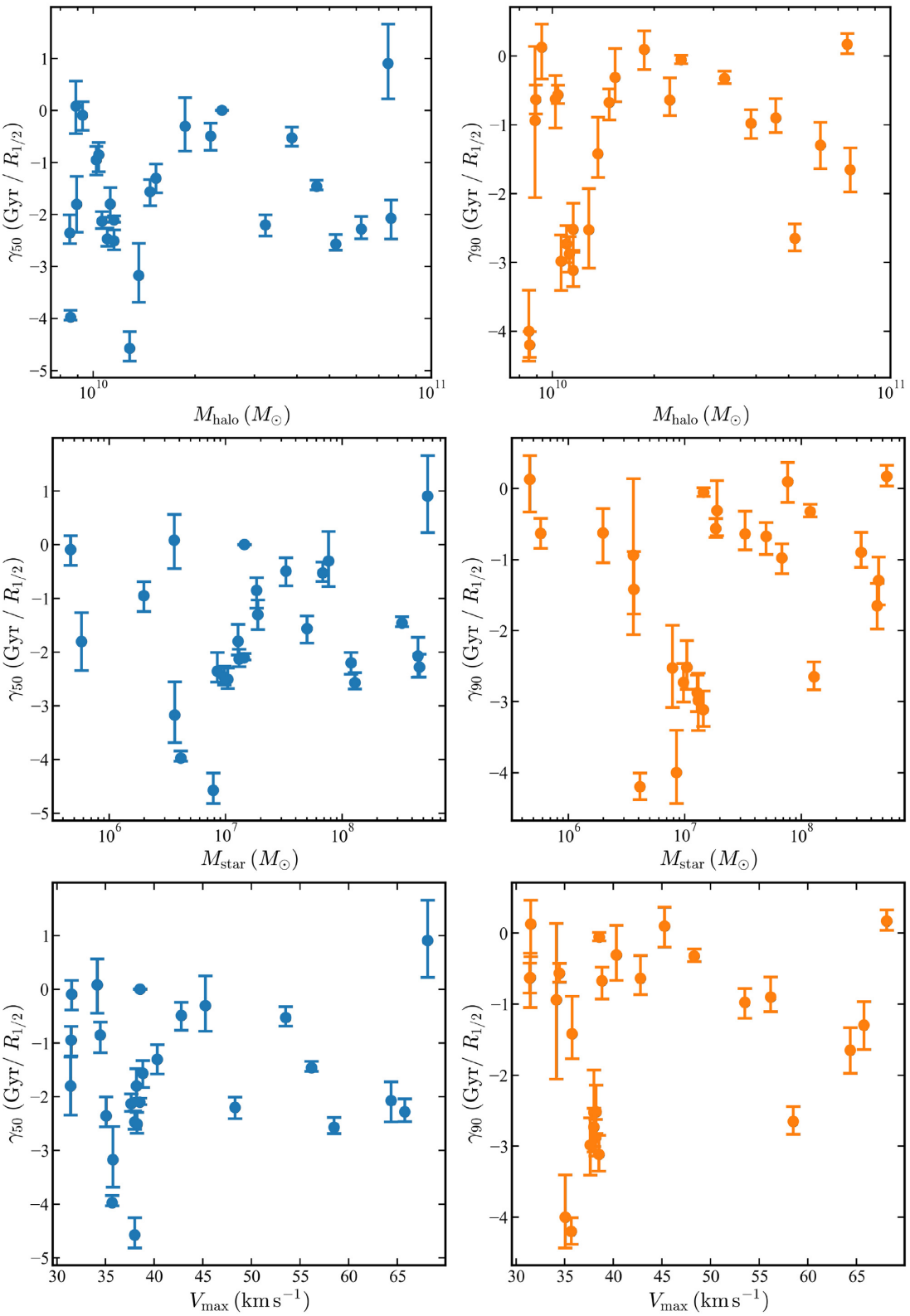

Figure A1. Age gradients for all of the galaxies in the sample, plotted against $M_{\rm vir}$ and $M_{\rm star}$. No trend is apparent. Note that the galaxies in the Fitts et al. (2017) sample were specifically selected to lie at $M_{\rm halo} = 10^{10}$ M$_\odot$.

APPENDIX B: REFERENCES FOR OBSERVED LOCAL GROUP DWARFS

Table B1 shows the properties of the observed dwarf galaxies.

Table B1. Observed properties for dwarf galaxies in the Local Group. This table only includes galaxies with $M_{\rm star} > 3.0 \times 10^3$ $M_\odot$, roughly the stellar mass of the smallest galaxy from the simulation suite used in this work. The columns are as follows: (1) galaxy name, (2) the galaxy host system divided between satellites of the Milky Way (MW), Satellites of Andromeda (And), and field galaxies, (3) the stellar mass of the galaxy, (4) the half-light radius of the galaxy, (5) the velocity dispersion of the galaxy, and (6) references for the half-light radii and velocity dispersions. The references are as follows: (1) McConnachie (2012), (2) van der Marel et al. (2002), (3) Harris & Zaritsky (2006), (4) Wolf et al. (2010), (5) Simon et al. (2006), (6) Geha et al. (2006), (7) Howley et al. (2012),(8) Geha et al. (2012), (9) Tollerud et al. (2012), (10) Ho et al. (2012), (11)Collins et al. (2013), (12) Cook et al. (1999), (13) Hunter & Elmegreen (2006),(14) Kirby et al. (2014), (15) Leaman et al. (2012), (16) Saviane, Held & Piotto (1996), and (17) Fraternali et al. (2009).

Galaxy Name	Host	$M_{\rm star}$ ($M_\odot$)	$r_{1/2}$ (pc)	σ_* km s^{-1}	reference
LMC	MW	1.1×10^9	–	$20.2^{+0.5}_{-0.5}$	1,2
SMC	MW	3.7×10^8	–	$27.6^{+0.5}_{-0.5}$	1,3
Fornax	MW	2.4×10^7	714^{+53}_{-53}	$10.7^{+0.2}_{-0.2}$	4
Leo I	MW	4.9×10^6	295^{+49}_{-49}	$9.0^{+0.4}_{-0.4}$	4
Sculptor	MW	3.9×10^6	282^{+41}_{-41}	$9.0^{+0.2}_{-0.2}$	4
Leo II	MW	1.2×10^6	177^{+13}_{-13}	$6.6^{+0.5}_{-0.5}$	4
Ursa Minor	MW	5.4×10^5	445^{+44}_{-44}	$11.5^{+0.6}_{-0.6}$	4
Sextans I	MW	7×10^5	768^{+47}_{-47}	$7.1^{+0.3}_{-0.3}$	4
Carina	MW	3.8×10^5	254^{+28}_{-28}	$6.4^{+0.2}_{-0.2}$	4
Draco	MW	3.2×10^5	220^{+11}_{-11}	$10.1^{+0.5}_{-0.5}$	4
CanVenI	MW	3×10^5	564^{+36}_{-36}	$7.6^{+0.5}_{-0.5}$	4
M33	And	4.7×10^9	2344^{+297}_{-297}	50^{+5}_{-5}	1,5
NGC 205	And	4.7×10^8	520^{+29}_{-29}	41^{+14}_{-14}	6
M32	And	4.1×10^8	110^{+16}_{-16}	$29.9^{+3.1}_{-2.9}$	7
NGC 147	And	9.9×10^7	364^{+24}_{-24}	16^{+1}_{-1}	8
NGC 185	And	6.8×10^7	358^{+16}_{-14}	24^{+1}_{-1}	8
And VII	And	1.5×10^7	977^{+46}_{-43}	13^{+1}_{-1}	9
And II	And	9.1×10^6	1340^{+45}_{-44}	$7.8^{+1.1}_{-1.1}$	10
And I	And	7.6×10^6	832^{+39}_{-37}	$10.2^{+1.9}_{-1.9}$	9
And III	And	1.8×10^6	$524^{+0.0}_{-0.0}$	$9.3^{+1.4}_{-1.4}$	9
And XXIII	And	1.7×10^6	1001^{+53}_{-52}	7.1^{+1}_{-1}	11
And VI	And	1.7×10^6	524^{+49}_{-49}	$12.4^{+1.5}_{-1.3}$	11
And XXI	And	1.1×10^6	1023^{+73}_{-68}	$7.2^{+5.5}_{-5.5}$	9
And XXV	And	1.1×10^6	642^{+47}_{-74}	$3.0^{+1.2}_{-1.1}$	11
LGS3	And	9.6×10^5	625^{+64}_{-61}	$7.9^{+5.3}_{-2.9}$	12
And XV	And	7.7×10^5	355^{+43}_{-38}	$4.0^{+1.4}_{-1.4}$	9
And V	And	6.2×10^5	446^{+21}_{-20}	$10.5^{+1.1}_{-1.1}$	9
And XIX	And	5.3×10^5	1481^{+62}_{-268}	$4.7^{+1.6}_{-1.6}$	11
And XIV	And	3.8×10^5	537^{+38}_{-35}	$5.3^{+1.0}_{-1.0}$	9
IC 1613	Field	1×10^8	1040^{+65}_{-65}	10.8^{+1}_{-1}	13,14
NGC 6822	Field	8.3×10^7	478^{+28}_{-28}	$23.2^{+1.2}_{-1.2}$	13,14
WLM	Field	3.9×10^7	1569^{+74}_{-74}	17.0^{+1}_{-1}	15
Pegasus	Field	6.6×10^6	695^{+37}_{-37}	$12.3^{+1.2}_{-1.1}$	13,14
Cetus	Field	4.5×10^6	612^{+38}_{-38}	8.3^{+1}_{-1}	13,14
Leo A	Field	3×10^6	354^{+19}_{-19}	$6.7^{+1.4}_{-1.2}$	13,14
Aquarius	Field	1.6×10^6	342^{+15}_{-15}	$7.9^{+1.9}_{-1.6}$	14
Tucana	Field	9×10^5	209^{+34}_{-34}	$15.8^{+4.1}_{-3.1}$	15,16
And XVIII	Field	8×10^5	416^{+30}_{-28}	$9.7^{+2.3}_{-2.3}$	9
And XVII	Field	3.5×10^5	262^{+53}_{-46}	$2.9^{+1.9}_{-2.2}$	11
And XXVIII	Field	3.4×10^5	210^{+60}_{-50}	$6.6^{+2.9}_{-2.1}$	11

This paper has been typeset from a TEX/LATEX file prepared by the author.